Automated Classification of Usual Interstitial Pneumonia Using Regional Volumetric Texture Analysis in High-Resolution Computed Tomography

Adrien Depeursinge, PhD,*† Anne S. Chin, MD,* Ann N. Leung, MD,* Donato Terrone, MD,*
Michael Bristow, MD,* Glenn Rosen, MD,* and Daniel L. Rubin, MD, MS*‡

Objectives: We propose a novel computational approach for the automated classification of classic versus atypical usual interstitial pneumonia (UIP).

Materials and Methods: Thirty-three patients with UIP were enrolled in this study. They were classified as classic versus atypical UIP by a consensus of 2 thoracic radiologists with more than 15 years of experience using the American Thoracic Society evidence–based guidelines for computed tomography diagnosis of UIP. Two cardiothoracic fellows with 1 year of subspecialty training provided independent readings. The system is based on regional characterization of the morphological tissue properties of lung using volumetric texture analysis of multiple-detector computed tomography images. A simple digital atlas with 36 lung subregions is used to locate texture properties, from which the responses of multidirectional Riesz wavelets are obtained. Machine learning is used to aggregate and to map the regional texture attributes to a simple score that can be used to stratify patients with UIP into classic and atypical subtypes.

Results: We compared the predictions on the basis of regional volumetric texture analysis with the ground truth established by expert consensus. The area under the receiver operating characteristic curve of the proposed score was estimated to be 0.81 using a leave-one-patient-out cross-validation, with high specificity for classic UIP. The performance of our automated method was found to be similar to that of the 2 fellows and to the agreement between experienced chest radiologists reported in the literature. However, the errors of our method and the fellows occurred on different cases, which suggests that combining human and computerized evaluations may be synergistic.

Conclusions: Our results are encouraging and suggest that an automated system may be useful in routine clinical practice as a diagnostic aid for identifying patients with complex lung disease such as classic UIP, obviating the need for invasive surgical lung biopsy and its associated risks.

Key Words: computer-assisted image processing, usual interstitial pneumonia, multidetector computed tomography, computer-assisted diagnosis

(*Invest Radiol* 2015;00: 00–00)

I diopathic pulmonary fibrosis (IPF) is a specific form of progressive fibrosing parenchymal pneumonia of unknown cause and is the leading cause of end-stage lung disease requiring transplantation accounting for more than 50% of lung transplants.[1] Median survival for patients with IPF remains dismal at 3 years after diagnosis.[2–4] Idiopathic pulmonary fibrosis is associated with the histologic and/or radiologic pattern of usual interstitial pneumonia (UIP).[5,6] Candidates for surgical biopsy must be carefully selected because the procedure is invasive as well as costly and carries significant risks in patients with possible UIP. Specifically, an acute exacerbation of their lung disease is an uncommon but potentially fatal complication after biopsy.[2] Surgical lung biopsy can be obviated when the clinical and radiographic impressions are typical of UIP.[7–10] However, atypical appearances of UIP are common, accounting for 30% to 50% of patients.[2,11] In this context, candidate selection for lung biopsy requires a multidisciplinary consensus of clinicians and radiologists experienced in interstitial lung diseases, found only in specialized centers of practice.

The classic computed tomographic (CT) appearance of UIP is characterized by basal- and peripheral-predominant reticular abnormality and honeycombing[2,12] (Table 1). Importantly, a confident CT diagnosis of UIP also requires the absence of atypical findings. The accurate identification of classic UIP requires meticulous characterization of parenchymal abnormalities as well as appropriate anatomic localization, mosty accurately performed by experienced thoracic radiologists.[13] The characterization of lung parenchymal abnormalities such as honeycombing, reticulation, and ground glass requires the appreciation of subtle 3-dimensional (3D) morphological tissue properties (eg, parenchymal texture) shown in Figure 1. A challenge is that visual inspection demonstrates low reproducibility.[14] The importance of relating these patterns to their anatomical location in the lungs (upper, middle, lower zones, etc) adds another level of complexity and is subject to high interobserver variation.

The automated computerized recognition of lung tissue types in chest CT has been an active research domain to assist image interpretation and enhance diagnosistic accuracy.[15] Most studies are based on 2-dimensional texture analysis on a slice basis.[16–19] Few studies fully leverage the wealth of 3D data contained in contemporary volumetric CT data sets, specifically using 3D solid texture analysis.[14,20,21] Even more infrequent is an approach that localizes tissue texture properties in the lung anatomy. The latter is of crucial importance, not only for the differential diagnosis of diffuse lung diseases but also because the typical appearance of most tissue types differs in distinct regions of the lung. The elaboration of a detailed digital atlas of the lungs is challenging mainly because of substantial intersubject variations in pulmonary architecture and breathing cycle, especially for patients with IPF in whom fibrotic architectural distortion is a characteristic feature. A digital lung tissue atlas based on intersubject 3D image registration has been proposed to overcome this challenge.[22] This approach has recently been refined with a landmark-based coordinate system,[23] which proved to be more robust to changes in structures across individuals. To our knowledge, this approach has not yet been used to characterize interstitial lung disease. Zrimec and Wong[24] developed a basic atlas to improve classification of honeycombing. However, their approach is based on peripheral lung regions only (neither vertical nor lateral characterization), which are analyzed with 2-dimensional texture features extracted on axial slices.

TABLE 1. Radiological Criteria for UIP[1]

Classic UIP (All Required)	Inconsistent With UIP (Any)
Peripheral, basal predominance	Upper or midlung predominance
Reticular abnormality	Peribronchovascular predominance
Honeycombing with or without traction bronchiectasis	Extensive ground-glass abnormality (extent > reticular abnormality)
Absence of features listed as inconsistent with UIP pattern	Profuse micronodules (bilateral, predominantly upper lobes)
	Discrete cysts (multiple, bilateral, away from areas of honeycombing)
	Diffuse mosaic attenuation/air trapping (bilateral, in 3 or more lobes)
	Consolidation in bronchopulmonary segment(s)/lobe(s)

UIP indicates usual interstitial pneumonia.

In this article, we used a basic anatomic atlas to define and extract morphological tissue properties (ie, 3D texture) from 36 anatomical subregions of the lung parenchyma. The latter were aggregated to create computational models of the radiological phenotypes for classic and atypical UIP. We hypothesized that the characterization of these radiologic phenotypes differentiates the UIP subtypes, specifically classic versus atypical UIP. To produce an automated system for this classification task, machine learning was used to derive a score from the regional texture attributes. This score identified patients with typical versus atypical UIP, the latter requiring further evaluation (eg, biopsy) to confirm the diagnosis of IPF. To the best of our knowledge, our work is the first attempt to automatically differentiate the UIP subtypes using computational methods.

MATERIALS AND METHODS

Data set

Computed tomographic examinations of 33 patients with biopsy-proven UIP/IPF from Stanford Hospital and Clinics were retrospectively reviewed. The examinations were performed in compliance with national legislation and Declaration of Helsinki guidelines, with institutional review board waiver of informed consent for this retrospective analysis. Two thoracic radiologists with more than 15 years of experience worked in consensus to classify each patient as classic versus atypical UIP on the basis of the American Thoracic Society evidence–based guidelines for CT diagnosis of IPF/UIP listed in Table 1.[1] There were 15 patients categorized as having a classic UIP and 18 patients with an atypical UIP appearance on CT. Additional readings were performed by 2 cardiothoracic fellows, each having 1-year specialty training to establish an optimal human performance. A volumetric CT scan was available for each patient, which was acquired within the year of the biopsy-proven diagnosis. The standard routine protocols yielded a computed tomographic dose index of 19.51 ± 8.81 mGy and a dose-length product of 622.11 ± 269.97 mGy·cm. The CT scans were reconstructed with slice thicknesses of 0.625 mm (1), 1 mm (15), 1.25 mm (14), and 2 mm (3). The spacings between the slices are 0.6 mm (3), 1 mm (13), 1.25 mm (14), as well as 2 mm (3), and the pixel spacings are in the range of 0.59 to 0.82 mm. All volumes were resampled to have isotropic cubic voxels of $0.59 \times 0.59 \times 0.59$ mm^3 using cubic spline interpolation. This ensures that the physical dimensions (ie, image scales and directions) are comparable between the patients.

3D Anatomical Atlas of the Lungs

A simple anatomical atlas of the lung served as a 3D reference to localize the various lung tissue types. The locations were chosen according to the predominant pattern sites of classic UIP (Table 1). First, a semiautomated segmentation of the lung volumes was carried out with a graphical user interface.[25] The user initiated a region growing algorithm from a seed point placed inside the lungs. The growing 3D region mimics the propagation of air in lungs, where each neighboring voxel is added to the region M_{lung} if the summed value of its own neighbors differs by less than a threshold value defined by the user. The lungs are divided vertically into apical, middle lung, and basal regions on the basis of the center of mass of M_{lung} (Table 2). The axial division results into central, intermediate, and peripheral lung regions. Left, right, anterior, and posterior regions are defined on the basis of the intersections of the coronal and sagittal planes. The intersections of all 10 lung divisions results in 36 subregions.

3D Texture Quantification Using Riesz Wavelets

Three-dimensional multiscale Riesz filter banks were used to characterize the morphological properties of the lung parenchyma in volumetric CT. These filters are advantageous for texture characterization because they quantify the local amount of directional image patterns at multiple scales. Second-order Riesz wavelets were used,[26,27] yielding 6 filters per image scale that are oriented along the main image directions *X*, *Y*, and *Z* as well as 3 diagonals *XY*, *XZ* and *YZ* (Fig. 2). Likewise, Riesz wavelets allow for a complete coverage of image scales and directions. We hypothesized that the local morpholgical tissue properties of the normal lung, ground glass, reticulation, and honeycombing can be expressed as the combinations of the responses of the oriented filters. The filters were implemented at multiple scales to analyze both fine morphological structures and coarser reticulations of the lung parenchyma.
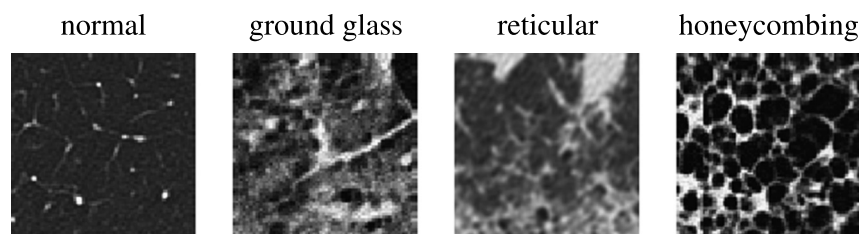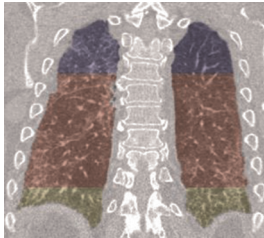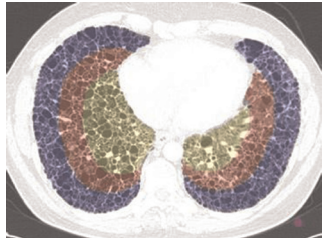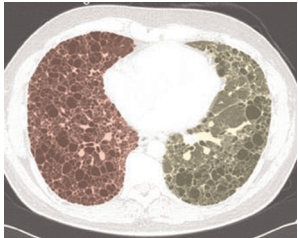
normal   ground glass   reticular   honeycombing
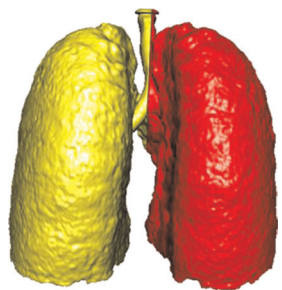
FIGURE 1. Common parenchymal appearances of UIP in CT.

TABLE 2. Localization of the Lung Masks

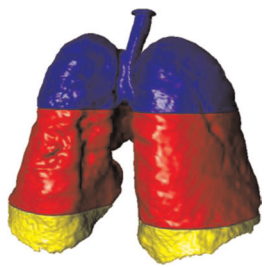| ⊥ **Vertical**	⊥ **Axial**	⊥ **Coronal**	⊥ **Sagittal**
Apical, central, basal	Peripheral, middle, axial	Left, right	Anterior, posterior

The lungs are split perpendicularly to 4 axes.[25]

Images can be viewed online in color at www.investigativeradiology.com.

Regional Lung Texture Analysis

The prototype regional distributions of the morphological tissue properties of classic versus atypical UIPs were learned using support vector machines (SVMs). The SVM is a supervised machine learning algorithm that can learn the complex relationship between a group of variables (ie, the vector v_l) and the presence or absence of a class from an ensemble of examples called the training set.[28] Once the SVM model has been built from the example cases, it can predict the class of an unseen case with a confidence score (called *computer score* thereinafter). The group of variables feeding SVMs consisted of the responses (ie, energies) of the multiscale Riesz filters in each of the 36 anatomical regions of the lungs (Fig. 3). The size of the vector v_l regrouping the responses of the 6 Riesz filters at 4 scales from the 36 regions was equal to 864.

To compare Riesz wavelets with other features that could capture the radiological phenotype of diffuse lung disease, 2 different feature groups were extracted for each region to provide a baseline performance: 15 histogram bins of the gray levels in the extended lung window [−1000; 600] Hounsfield units (HU) and 3D gray-level co-occurrence matrices (GLCM).[29] Statistical measures from GLCMs are popular texture attributes that were used by several studies in the literature to characterize the morphological properties of lung tissue associated with interstitial lung diseases.[16,17,20,21] They consist in counting the co-occurrence of voxels with identical gray level values that are separated by a distance d, which results in a co-occurrence matrix. Eleven statistics were extracted from these matrices[29] as texture attributes. The choices of d and the number of gray levels were optimized by considering values in {−3; 3} and {8, 16, 32}, respectively. The size of the vector of attributes v_l was 540 for the gray-level histogram attributes (called *HU* thereinafter) and 396 for the GLCM attributes.

RESULTS

A leave-one-patient-out cross-validation evaluation was used to estimate the performance of the proposed approach. The leave-one-patient-out cross-validation consisted of using all patients but 1 to train the SVM model and to measure the prediction performance on the remaining test patient. The prediction performance was then averaged over all possible combinations of training and test patients. Receiver operating characteristic (ROC) curves of the system's performance in classifying between classic and atypical UIP are shown in Figure 4 for different feature groups and their combinations. The ROC curves were obtained by varying the decision threshold between the minimum and
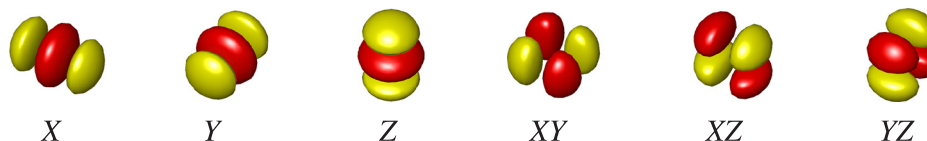

FIGURE 2. Second-order Riesz filters characterizing edges along the main image directions *X, Y, Z* and 3 diagonals *XY, XZ,* and *YZ*. Figure 2 can be viewed online in color at www.investigativeradiology.com.
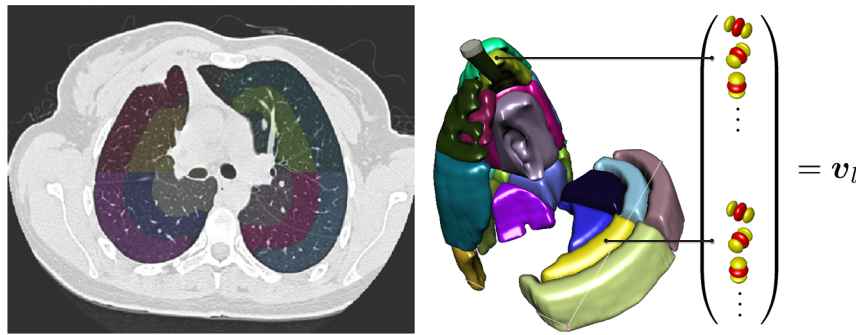
FIGURE 3. The 36 subregions of the lungs localized the prototype regional distributions of the texture properties. Figure 3 can be viewed online in color at www.investigativeradiology.com.

the maximum of the score provided by the SVMs. A maximum area under the ROC curve (AUC) of 0.81 was obtained with the regional Riesz attributes, which suggests that prediction was correct for more than 4 of 5 patients. The performance of HU and GLCM attributes was close to random (0.54 and 0.6 for HU and GLCMs, respectively). On the other hand, predictive SVM models based on the responses of the Riesz filters, averaged over the entire lungs, had an AUC of 0.72.

Our system's performance was also compared with the interpretations of 2 fellowship-trained cardiothoracic fellows, each having 1 year of experience. Interobserver agreement was assessed with the Cohen κ statistics[30] and the percentage of agreement (ie, number of times the 2 observer agreed). The comparisons are detailed in Tables 3 and 4. The operating points of the 2 independent observers are reported in Figure 4 (top right). A detailed analysis of the 6 cases that were misclassified by our system is shown in Table 5 with representative CT images, including predictions from the computer and the 2 fellows compared with the consensus classification. The system predicted 2 classic UIP cases as atypical UIP and 3 atypical UIP cases as classic UIP. A comprehensive analysis of all 33 cases is illustrated in the Supplemental Table, Supplemental Digital Content 1, http://links.lww.com/RLI/A189.

Overall, 7 incorrect predictions were made by the fellows and 6 incorrect predictions by the computer. The fellows and the computer made only 2 common errors (cases 1 and 13).

DISCUSSION

We developed a novel computational method for the automated classification of classic versus atypical UIP based on regional volumetric texture analysis. This constitutes, to the best of our knowledge, a first attempt to automatically differentiate the UIP subtypes with computational methods. An SVM classifier yielded a score that predicts if the UIP is classic or atypical. The classifier was based on a group of attributes that characterize the radiological phenotype of the lung parenchyma, specifically the morphological properties (ie, texture) of the parenchyma. Because diffuse lung diseases can vary in the distribution and severity of abnormalities throughout the lungs, we extracted our quantiative image features from 36 anatomical regions of the lung. To our knowledge, adding this spatial characterization to the computational model is also innovative, and it is particularly relevant for assessing diffuse lung disease.
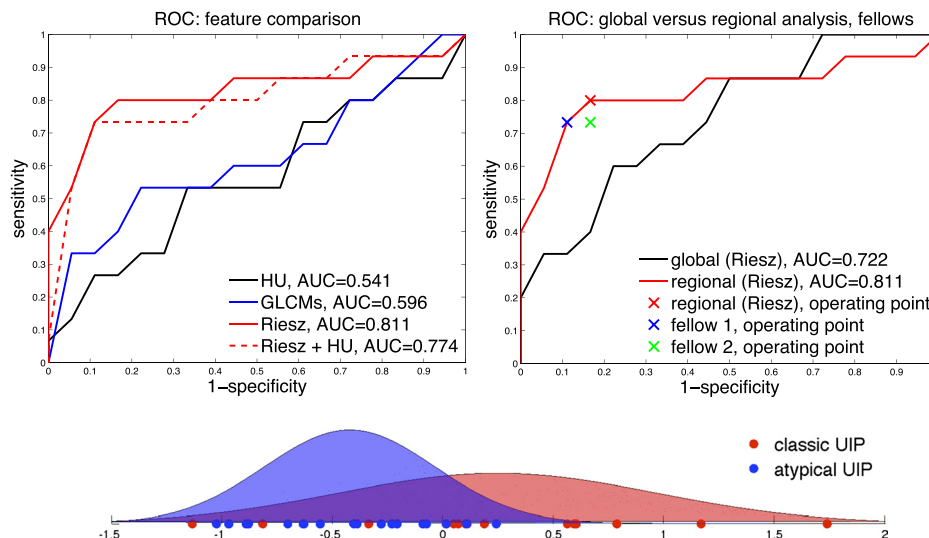

FIGURE 4. The ROC analysis of the system's performance. Classic UIP is the positive class. Left, Comparison of various feature groups using the digital lung tissue atlas. Three-dimensional Riesz wavelets provide a superior AUC of 0.81. Right, Importance of the anatomical atlas when compared with an approach based on the global tissue properties and comparison of the computer's and cardiothoracic fellows' performance. Bottom, Probability density functions of the computer score for classic (red) and atypical UIP (blue) based on regional Riesz texture analysis and the computer's operating point highlighted in the upper right subfigure. Atypical UIP is associated with a negative score, which implies that positive scores predict classic UIPs with high specificity. Figure 4 can be viewed online in color at www.investigativeradiology.com.

TABLE 3. Interobserver Agreement (Cohen κ Statistics)

Cohen κ	Consensus	Fellow 1	Fellow 2	Computer (Regional Riesz Texture Analysis)
Consensus	1	—	—	—
Fellow 1	0.629	1	—	—
Fellow 2	0.569	0.9374	1	—
Computer (regional Riesz)	0.633	0.506	0.569	1

System Performance and Comparison With Chest Specialists

The proposed approach successfully predicted UIP subtypes for more than 4 of 5 patients (AUC, 0.81), with high specificity for classic UIPs. This performance is encouraging and suggests that an automated system may be useful in routine clinical practice for radiologists with limited experience in interpretation of diffuse lung diseases. The detailed case analyses (see Supplemental Table, Supplemental Digital Content 1, http://links.lww.com/RLI/A189) reveal that, with the exception of 1 case (case 20), the computer score was able to sort and grade the patients from highly atypical (eg, patients 2 and 3) to classic (eg, patient 33). The observer agreement between the computer and the consensus was associated with a κ value of 0.63 and a percentage of agreement of 81.82, which is considered as being substantial in the literature.[31] The performance of the computer was found to be comparable with that of the cardiothoracic fellows with 1 year of specialty training (Fig. 4, top right). The agreement between each of the 2 fellows and the computer was moderate (ie, 0.51 and 0.57 κ values and 75.8% and 78.8% agreement) when compared with their excellent interreader agreement (ie, κ value and percentage of agreeement of 0.94 and 97%, respectively). However, the agreement between each of the fellows with the consensus classification (our criterion standard) is considerably lower (ie, 0.63 and 0.57 κ values and 81.8% and 78.8% agreement). Interestingly, the agreement between the computer and the consensus was comparable with the agreement between the fellows and the consensus, suggesting that, although the algorithm can still be improved in terms of agreement with the consensus, the current method performs at least as well as cardiothoracic fellows. The performance was also consistent with the interreader agreement between the 2 expert radiologists (ie, 4 and 8 years of experience, κ value of 0.67) reported by Assayag et al[13] in their study. Because the target application for this algorithm is for general radiologists, the proposed system could considerably improve their performance, a study which we plan to undertake.

Detailed Case Analysis of the System's Performance

Our cohort had a much higher proportion of atypical UIPs accounting for more than half the cases, which likely reflects a selection bias. In current practice, only cases that are atypical have histologic/pathologic confirmation, which was required for this cohort analysis. Many of the cases had subtle findings that required adhering very strictly to the guidelines for classification by the consensus, which may account for 3 of 6 erroneous predictions of atypical UIP by the computer (see Table 5 and the Supplemental Table, Supplemental Digital Content 1, http://links.lww.com/RLI/A189). We believe that the algorithm would perform better in a real-world setting, which does not reflect unusual cases referred to a quaternary academic institution.

Erroneous predictions of classic UIP by the computer occurred in 2 patients (patients 24 and 27) where bronchiectasis was mistaken for honeycombing (Table 5). This can be a difficult task even for experienced chest radiologists, but it will constitute a target for further improvement of the system. One patient with diffuse disease without definite basilar predominance was also misclassified as classic UIP by the computer.

Overall, 7 incorrect predictions were made by the cardiothoracic fellows and 6 incorrect predictions by the computer. Combining these predictions results in only 2 incorrect predictions of 33 (ie, 94% correct predictions), demonstrating the potential benefit of computer-assisted diagnosis in the setting of UIP.

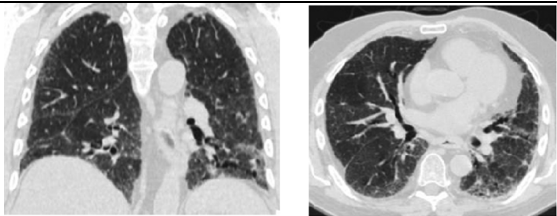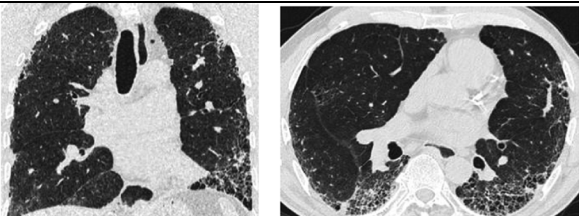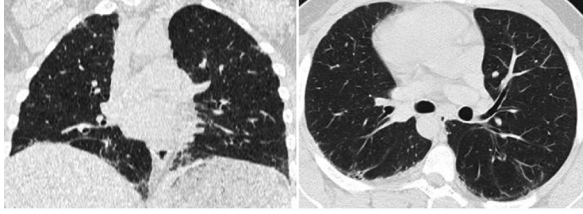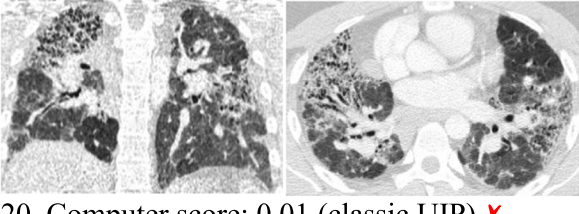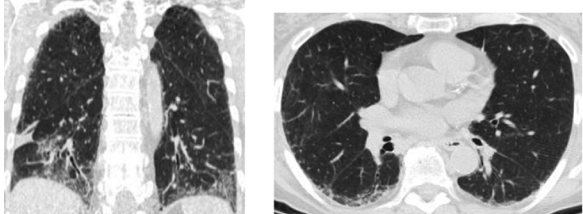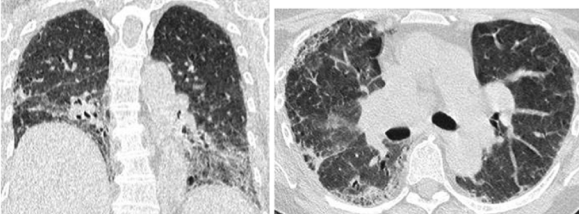## Comparison of the Quantitative Image Features

The gray-level histograms (ie, HU) failed to predict the UIP subtypes, and 3D GLCMs provided a slightly better specificity for classical UIPs. The 3D Riesz wavelets provided an AUC of 0.81, which was found to be higher than that of 3D GLCMs and HU. The combination of Riesz and HU did not lead to a performance improvement. This can be explained by the fact that the distinction between tissue types associated with UIP requires a fine characterization of the volumetric morphological tissue properties (ie, 3D texture) that only 3D Riesz wavelets were able to extract. The prototype gray-level distributions of ground glass, reticular, and honeycombing may not be sufficiently distinct to accurately discriminate among them, as shown in Figure 1. The comparison between global and regional texture analysis (Fig. 4, right) highlights the importance of localizing tissue texture properties, which is consistent with the medical knowledge.[1]

Overall, we believe that our automated system may be useful in general radiology practices, accounting for the majority of sites where patients with IPF are initially examined, to accurately identify patients with classic UIP for which an unnecessary surgical biopsy can be avoided. The high-resolution imaging of lung disease afforded by modern-day CT provides accurate 3D anatomic/pathologic fidelity in patients with classic UIP features. A confident CT diagnosis of classic UIP can eliminate the need for an invasive surgical biopsy to confirm this diagnosis; this underscores the importance of an accurate and reliable interpretation of the CT examination. This task is often challenging, particularly in less-specialized practice centers without access to

TABLE 4. Interobserver Agreement (Percentage of Times That the Observers Agreed)

% Agreement	Consensus	Fellow 1	Fellow 2	Computer (Regional Riesz Texture Analysis)
Consensus	100	—	—	—
Fellow 1	81.82	100	—	—
Fellow 2	78.79	96.97	100	—
Computer (regional Riesz)	81.82	75.76	78.79	100

TABLE 5. Detailed Analysis of the 6 Cases That Were Missclassified by Our System

1. Computer score: -1.13 (atypical UIP) ✗

   consensus: classic UIP

   fellow 1: atypical UIP ✗

   fellow 2: atypical UIP ✗

6. Computer score: -0.82 (atypical UIP) ✗

   consensus: classic UIP

   fellow 1: classic UIP ✓

   fellow 2: classic UIP ✓

13. Computer score: -0.34 (atypical UIP) ✗

    consensus: classic UIP

    fellow 1: atypical UIP ✗

    fellow 2: atypical UIP ✗

20. Computer score: 0.01 (classic UIP) ✗

    consensus: atypical UIP

    fellow 1: atypical UIP ✓

    fellow 2: atypical UIP ✓

24. Computer score: 0.1 (classic UIP) ✗

    consensus: atypical UIP

    fellow 1: atypical UIP ✓

    fellow 2: atypical UIP ✓

27. Computer score: 0.24 (classic UIP) ✗

    consensus: atypical UIP

    fellow 1: atypical UIP ✓

    fellow 2: classic UIP ✗

Coronal and axial views of the lung parenchyma in computed tomographic scans are shown with a window level of −500 HU and a width of 1400 HU.
UIP indicates usual interstitial pneumonia.
Images can be viewed online in color at www.investigativeradiology.com.

experts experienced in interstitial lung disease. Nevertheless, reduction of needless invasive biopsies is desired when possible to reduce costs and, more importantly, to avoid unnecessary morbidity/mortality in patients with UIP. We recognize several limitations of the current work, including the small number of cases included in the study and the use of a very simple digital atlas of the lung anatomy. Future work will include validating our results in an independent data set and performing regional learning of 3D rotation-covariant texture models of normal, ground glass, reticular, and honeycombing.[27,31]

REFERENCES

1. Raghu G, Collard HR, Egan JJ, et al. An official ATS/ERS/JRS/ALAT statement: idiopathic pulmonary fibrosis: evidence-based guidelines for diagnosis and management. *Am J Respir Crit Care Med*. 2011;183:788–824.

2. Lynch DA, Huckleberry JM. Usual interstitial pneumonia: typical and atypical high-resolution computed tomography features. *Semin Ultrasound CT MR*. 2014;35:12–23.

3. Sumikawa H, Johkoh T, Colby TV, et al. Computed tomography findings in pathological usual interstitial pneumonia: relationship to survival. *Am J Respir Crit Care Med*. 2008;177:433–439.

4. Alhamad EH, Al-Kassimi FA, AlBoukai AA, et al. Comparison of three groups of patients with usual interstitial pneumonia. *Respir Med*. 2012;106:1575–1585.

5. Lynch JP, Saggar R, Weigt SS, et al. Usual interstitial pneumonia. *Semin Respir Crit Care Med*. 2006;27:634–651.

6. Johkoh T, Sumikawa H, Fukuoka J, et al. Do you really know precise radiologic-pathologic correlation of usual interstitial pneumonia? *Eur J Radiol*. 2014;83: 20–26.

7. Flaherty KR, King TE, Raghu JG, et al. Idiopathic interstitial pneumonia: what is the effect of a multidisciplinary approach to diagnosis? *Am J Respir Crit Care Med*. 2004;170:904–910.

8. Gogali A, Wells AU. Diagnostic approach to interstitial lung disease. *Curr Respir Care Rep*. 2012;1:199–207.

9. Gruden JF, Panse PM, Leslie KO, et al. UIP diagnosed at surgical lung biopsy, 2000-2009: HRCT patterns and proposed classification system. *Am J Roentgenol*. 2013;200:458–467.

10. Aaløkken TM, Naalsund A, Mynarek G, et al. Diagnostic accuracy of computed tomography and histopathology in the diagnosis of usual interstitial pneumonia. *Acta Radiol*. 2012;53:296–302.

11. Raghu G, Lynch D, Godwin D, et al. Diagnosis of idiopathic pulmonary fibrosis with high-resolution CT in patients with little or no radiological evidence of honeycombing: secondary analysis of a randomised, controlled trial. *Lancet Respir Med*. 2014;2:277–284.

12. Hunninghake GW, Lynch DA, Galvin JR, et al. Radiologic findings are strongly associated with a pathologic diagnosis of usual interstitial pneumonia. *Chest*. 2003;124:1215–1223.

13. Assayag D, Elicker BM, Urbania TH, et al. Rheumatoid arthritis-associated interstitial lung disease: radiologic identification of usual interstitial pneumonia pattern. *Radiology*. 2014;270:583–588.

14. Depeursinge A, Foncubierta-Rodríguez A, Van De Ville D, et al. Three-dimensional solid texture analysis and retrieval in biomedical imaging: review and opportunities. *Med Image Anal*. 2014;18:176–196.

15. Sluimer IC, Schilham A, Prokop M, et al. Computer analysis of computed tomography scans of the lung: a survey. *IEEE Trans Med Imaging*. 2006;25:385–405.

16. Park YS, Seo JB, Kim N, et al. Texture-based quantification of pulmonary emphysema on high-resolution computed tomography: comparison with density-based quantification and correlation with pulmonary function test. *Invest Radiol*. 2008;43:395–402.

17. Delorme S, Keller-Reichenbecher MA, Zuna I, et al. Usual interstitial pneumonia: quantitative assessment of high-resolution computed tomography findings by computer-assisted texture-based image analysis. *Invest Radiol*. 1997;32:566–574.

18. Yoon RG, Seo JB, Kim N, et al. Quantitative assessment of change in regional disease patterns on serial HRCT of fibrotic interstitial pneumonia with texture-based automated quantification system. *Eur Radiol*. 2013;23:692–701.

19. Guo J, Reinhardt JM, Kitaoka H, et al. Integrated system for CT-based assessment of parenchymal lung disease. Paper presented at: IEEE International Symposium on Biomedical Imaging; July 7–10, 2002; Washington, DC.

20. Korfiatis PD, Karahaliou AN, Kazantzi AD, et al. Texture-based identification and characterization of interstitial pneumonia patterns in lung multidetector CT. *IEEE Trans Inf Technol Biomed*. 2010;14:675–680.

21. Xu Y, Sonka M, McLennan G, et al. MDCT-based 3D texture classification of emphysema and early smoking related lung pathologies. *IEEE Trans Med Imaging*. 2006;25:464–475.

22. Li B, Christensen GE, Hoffman EA, et al. Establishing a normative atlas of the human lung: intersubject warping and registration of volumetric CT images. *Acad Radiol*. 2003;10:255–265.

23. Li B, Christensen GE, Hoffman EA, et al. Establishing a normative atlas of the human lung: computing the average transformation and atlas construction. *Acad Radiol*. 2012;19:1368–1381.

24. Zrimec T, Wong JSJ. Improving computer aided disease detection using knowledge of disease appearance. Paper presented at: 12th World Congress on Health (Medical) Informatics; August 20–24, 2007; Brisbane, Australia.

25. Depeursinge A, Zrimec T, Busayarat S, et al. 3D lung image retrieval using localized features. Paper presented at: SPIE Medical Imaging 2011: Computer-Aided Diagnosis; February 12–17, 2011; Orlando, FL.

26. Chenouard N, Unser M. 3D steerable wavelets and monogenic analysis for bioimaging. Paper presented at: IEEE International Symposium on Biomedical Imaging: from Nano to Macro; March 30, – April 2, 2011; Chicago, IL.

27. Depeursinge A, Foncubierta-Rodríguez A, Vargas A, et al. Rotation-covariant texture analysis of 4D dual-energy CT as an indicator of local pulmonary perfusion. Paper presented at: IEEE International Symposium on Biomedical Imaging: From Nano to Macro; April 7–11, 2013; San Francisco, CA.

28. Cortes C, Vapnik V. Support-vector networks. *Mach Learn*. 1995;20:273–297.

29. Kurani AS, Xu DH, Furst J, et al. Co-occurrence matrices for volumetric data. Paper presented at: IASTED International Conference on Computer Graphics and Imaging; August 17–19, 2004; Kauai, HI.

30. Viera AJ, Garett JM. Understanding interobserver agreement: the kappa statistic. *Fam Med*. 2005;37:360–363.

31. Depeursinge A, Foncubierta-Rodríguez A, Van De Ville D, et al. Rotation-covariant texture learning using steerable Riesz wavelets. *IEEE Trans Image Process*. 2014;23:898–908.